Characterization of the Spontaneous "Aging" of the Heme Oxygenase from the Pathological Bacterium *Neisseria meningitidis* via Cleavage of the C-Terminus in Contact with the Substrate. Implications for Functional Studies and the Crystal Structure†

Yangzhong Liu,‡ Li-Hua Ma,‡ Xuhong Zhang,§ Tadashi Yoshida,§ James D. Satterlee,|| and Gerd N. La Mar*,‡

Department of Chemistry, University of California, Davis, California 95616, Department of Biochemistry, Yamagata University School of Medicine, Yamagata 990-9585, Japan, and Department of Chemistry, Washington State University, Pullman, Washington 99164

Received November 10, 2005; Revised Manuscript Received December 29, 2005

ABSTRACT: Solution ^{1}H NMR spectroscopy and mass spectrometry are utilized to characterize the irreversible "aging" of native heme oxygenase from *N. meningitidis*, *Nm*HO. 2D NMR characterization of the cyanide-inhibited substrate complex shows that the C-terminal interaction between Arg208His209 and the exposed pyrrole of the protohemin substrate in the "native" *Nm*HO complex is lost in the "aging". Mass spectrometry and N-terminal sequencing of wild type and "aged" *Nm*HO reveal that the "aging" process involves cleavage of the Arg208His209 dipeptide. The construction of the double deletion mutant without Arg208His209 and its NMR comparison as both the resting state substrate complex and its cyanide-inhibited complex with the "aged" *Nm*HO reveal that cleavage of the C-terminal dipeptide is the only modification during the aging. Comparison of cyanide ligand binding constants reveal a factor ∼1.7 greater CN^- affinity in the native than "aged" *Nm*HO. The rate of protohemin degradation and its stereoselectivity are unaffected by the C-terminal truncation. However, the free α-biliverdin yield in the presence of desferrioxamine is significantly increased in the "aged" *Nm*HO and its deletion mutant relative to WT, arguing for a role of the *Nm*HO C-terminus in modulating product release. The facile cleavage of Arg208His209 in the resting state complex, with a half-life of ∼24 h at 25 °C, suggests that previous characterization of *Nm*HO may have been carried out on a mixture of native and "aged" *Nm*HO, and may account for the "lost" C-terminal residues in the crystal structures.

The pathological bacterium *Neisseria meningitidis* utilizes a heme oxygenase, HO[1] (named *Nm*HO, also HemO (*1*)), for securing the iron needed for host infection. Similarly sized, soluble HOs (∼210 residues) have been identified in numerous other bacteria, including those from *Corynebacterium diphtheriae* (*Cd*HO) (*2*) and *Pseudomonas aeruginosa* (*Pa*HO) (*3*). The bacterial HOs exhibit variable sequence homology among themselves and with the more extensively studied mammalian HOs (*4*−*6*). The latter HOs are larger (∼300 residues) and membrane-bound, but expression of truncated, soluble constructs where the C-terminal membrane anchor helix is deleted (*7*−*9*) yields soluble HOs with conserved activity. The various HOs appear to share a common mechanism, worked out for human (hHO) and rat (rHO) enzymes (*4*, *5*, *9*−*12*), where the reactive ferric hydroperoxy (*13*) species stereoselectively hydroxylates one protohemin (PH: Figure 1) meso position, which, with sequential O_2 and electrons, forms verdoheme and ferric-biliverdin as degradation intermediates (Scheme 1). Reduction of the iron in the latter intermediate results in loss of iron, followed by slow (∼0.03 s^{-1}) dissociation of the product biliverdin (*9*). In mammals, this very slow dissociation step is strongly accelerated by forming a transient 1:1 complex with biliverdin reductase, BVR, with the BVR:HO contact near the exposed pyrrole of the substrate/product (*14*).

The physiologically relevant, ferrous HO−substrate complex of O_2 or the ferric hydroperoxy species are, with one notable exception (*15*), insufficiently stable for detailed crystallographic or solution NMR structural studies. This has necessitated the use of the ferrous NO and CO, or ferric CN^-, N_3^-, or OH^- derivatives as model complexes. Crystal structures of both mammalian (*16*−*19*) and bacterial (*15*, *20*−*24*) HO−PH complexes reveal a common fold, despite their variation in sequence, with a mobile distal helix placed close to the substrate protohemin, PH (Figure 1), so as to block all but one of the four meso positions to electrophilic

† This work was supported, in part, by the National Institutes of Health, GM62830 (G.N.L.), GM47645 (J.D.S.), and a Grant-in-Aid for Scientific Research (16570102) from the Ministry of Education and Sports, Science and Teaching, Japan (T.Y.).

* Corresponding author: Department of Chemistry, University of California, Davis, One Shields Avenue, Davis, CA 95616. Phone: (530) 752-0958. Fax: (530) 752-8995. E-mail: lamar@chem.davis.edu.

‡ University of California.

§ Yamagata University School of Medicine.

|| Washington State University.

[1] Abbreviations: HO, heme oxygenase; *Nm*HO, *Neisseria meningitidis* heme oxygenase; ΔC2-*Nm*HO, *Neisseria meningitidis* heme oxygenase with Arg208/His207 deleted; *Pa*HO, *Pseudomonas aeruginosa* heme oxygenase; DSS, 2,2-dimethyl-2-silapentane-5-sulfonate; NOESY, two-dimensional nuclear Overhauser spectroscopy; TOCSY, two-dimensional total correlation spectroscopy; ROESY, two-dimensional rotating frame nuclear Overhauser spectroscopy.

10.1021/bi0523097 CCC: $33.50
Published on Web 03/02/2006

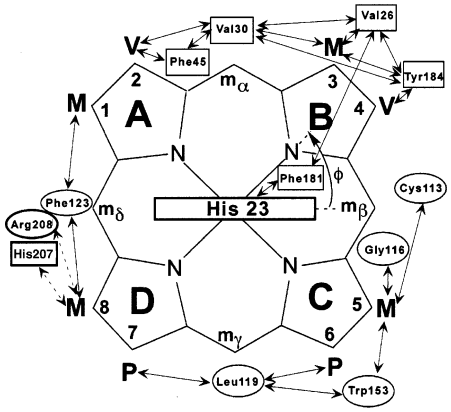

FIGURE 1: Structure of heme pocket of *Nm*HO−PH−CN in solution as based on dipolar contacts between the protoheme substrate and a series of sequence specifically assigned heme pocket residues. Only seven key residues are shown, with rectangles and circles representing key proximal and distal residues, respectively. The two residues His *I* (207) (proximal) and Arg208 (distal), shown in bold, make contact with pyrrole D (dashed lines) only in the initially prepared or WT $NmHO^{A}$−PH complex. Upon conversion to the $NmHO^{X}$−PH complex, the pyrrole D contacts to His *I* (207) and Arg208 are lost.

attack by the hydroperoxide (*9*, *12*). The distal helix backbone sterically orients all axial ligands (and presumably the hydroperoxide) toward the sole "open" meso position. A series of distal ordered water molecules were also detected (*15*, *17*, *18*, *20*−*23*, *25*) in all HO complexes and proposed to stabilize the unusual hydroperoxy complex (*12*). The common seating of PH in HOs leads to unique α-meso cleavage (*9*) in all but *Pa*HO, (*23*, *26*) where a 90° in-plane rotation of PH relative to PH in other HOs leads primarily to *δ*-meso cleavage. Solution NMR studies have shown that common heme orientational isomerism about the α-, *γ*-meso axis (*27*−*30*), and more novel, dynamic, in-plane rotational isomerism (*26*, *31*, *32*), are natural characteristics of HO−substrate complexes and that the ordered distal water molecules (*29*, *30*, *33*, *34*) are embedded in an extended H-bond network that involves some remarkably strong H-bonds.

None of the crystal structures of HOs have detected (*15*, *17*, *18*, *20*−*23*, *25*) the N- and C-terminal residues, with these "missing" residues attributed to disorder, as is common to the majority of crystal structures. In the case of *Nm*HO, however, it was noted (*20*, *21*) that the "missing" C-terminal residues could be placed closer to the substrate binding site than in other HOs. Solution ^{1}H NMR studies of the cyanide-ligated substrate complex of *Nm*HO have confirmed (*30*) a conserved molecular structure relative to that in crystals (*20*), with several residues, and one PH propionate, exhibiting alternate orientations depending on whether an H-bond donor (*20*) (H_2O) or an H-bond acceptor (*21*) (NO, CN^-) is ligated to the iron. A notable difference between the *Nm*HO−PH−CN solution structure (*30*) and either the *Nm*HO−PH−H_2O or *Nm*HO−PH−NO crystal structures (*20*, *21*) is that the former detects a direct interaction between one of the C-terminal His and pyrrole D (Figure 1) of the PH substrate. A simple model suggested (*30*) that Arg208 forms a salt bridge with the 7-propionate of the heme, with the His ring possibly H-bonding the Asp27 carboxylate. While the C-terminus clearly interacts with substrate in solution, the details as to which C-terminal His (207 or 209) interacts with the heme, as well as the nature of this interaction, are not yet clear.

We noted earlier (*30*) that, in solution, the initially prepared *Nm*HO−PH−CN or *Nm*HO−PH−H_2O, described as the "A" form, spontaneously, homogeneously, but irreversibly, convert into another species, referred to as the "X" form, with altered heme hyperfine shifts in substrate complexes. Our interest here is to characterize the nature of the structural change that accompanies this "A" → "X" transition due to "aging" in the physiologically relevant, resting state, high-spin ferric complex, *Nm*HO−PH−H_2O. However, strong relaxation obscures the majority of the key active site residues of interest in this complex, although even the simple spectrum of this complex allows detection of the formation of "X" (see below). Hence, we will structurally characterize the "aged" complex trapped as the low-spin, cyanide-inhibited complex, *Nm*HO−PH−CN, which provides the narrow NMR lines needed for definitive assignment and structural characterization and exhibits hyperfine shifts readily interpreted in terms of details of the active site molecular structure (*30*, *33*, *35*). ^{1}H NMR assignment of the majority of the relevant active site residues for the "A" form of *Nm*HO−PH−CN has been reported (*30*).

In this study, we revisit this "A" → "X" conversion to characterize by ^{1}H NMR the nature of the structural change that accompanies this conversion and to assess the relationship of this conversion to the interaction between the C-terminus and the substrate. We rely on ^{1}H NMR to demonstrate that the "A" → "X" conversion results in the loss of the C-terminal interaction with the substrate, and we rely on mass spectrometry to demonstrate that the "A" → "X" conversion entails a cleavage of the C-terminal Arg208 and His209 residues. We further show that this loss of the C-terminal interaction with substrate results in perturbed ligand affinity for the substrate iron and product biliverdin release, arguing for a functional role of the C-terminus in modulating heme reactivity. The detailed mechanism of the peptide cleavage in the *Nm*HO "A" → "X" conversion is yet to be determined, but a half-life of as short as 1 day for

Scheme 1

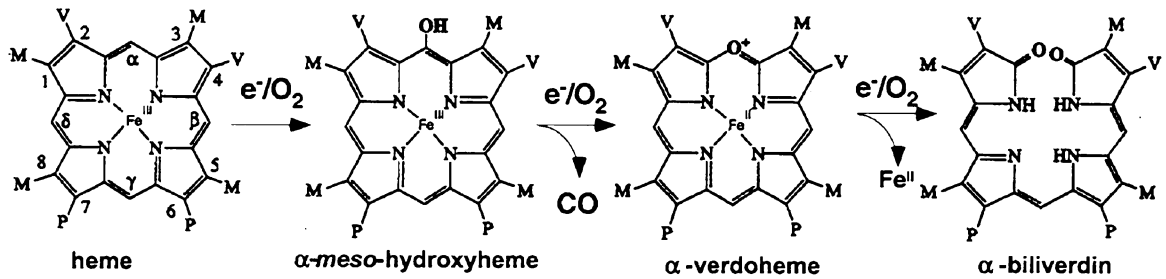

the "A" → "X" conversion is observed. Hence the facility of this "A" → "X" conversion for *Nm*HO suggests the possibility that structural and functional characterization for *Nm*HO and its substrate complexes may have been, or is being, performed on variable mixtures of the "A" and "X" form, or possibly, on primarily the "X" form. We emphasize here the elucidation of the structural difference in the "A" vs "X" species and identify a simple analytic marker for species "X".

EXPERIMENTAL PROCEDURES

Protein Preparation. The WT apo *Nm*HO samples utilized in this study are the same as those described in detail previously (*30*). All samples were kept frozen at −80 °C until required. Stoichiometric amounts of hemins were added to apo *Nm*HO in phosphate buffer (100 mM or 50 mM, pH 7.0). The substrate complex was purified by column chromatography on Sephadex G25 and concentrated to 1−3 mM by ultrafiltration. KCN buffered at pH 7.0 was added in ∼10-fold excess to prepare the cyanide complex, *Nm*HO−PH−CN. ^2H_2O for ^1H_2O solvent exchange was carried out by column chromatography (*36*).

The plasmid for the two C-terminal residue deletion mutant, named ΔC2-*Nm*HO, with Arg208 and His209 absent, was constructed as follows. PCR was carried out with an *Nm*HO expression vector, *Nm*HO (*30*) (formerly pMWHemO), as a template and a synthetic nucleotide F and ΔC2R as primers. The nucleotide F (5′-AATACGACTCAC-TATAGGGAGACCACAAC-3′) corresponds to the nucleotide sequence positions from −79 to −51 of pMW172, and the nucleotide ΔC2R (3′-GGCCTTCCTTACTACGGCGT-GATCGTGATTCGAATCCGGTGTTCA-5′) corresponds to the complementary nucleotide sequence positions from 607 to 644 of pMW*Nm*HO, except that the 3′-TCC-5′ codon for Arg208 was changed to 3′-ATC-5′ to create a stop codon. The second A in the *Nde*I recognition site, CATATG, is defined as +1. The target fragment was cut with *Nde*I and *Hin*dIII, and ligated into pMW172 to construct pMW*Nm*HOΔC2. Expression and purification of the ΔC2-*Nm*HO mutant were similar to those described for wild-type enzyme.

Samples of WT *Nm*HO−PH−H_2O were "aged" in ^1H_2O solution, 50 mM in phosphate, and pH 7.0 at 25 °C for 5−160 h. The "aging" was monitored by mass spectrometry and ^1H NMR as either the *Nm*HO−PH−H_2O or, for structural characterization, the cyanide-trapped *Nm*HO−PH−CN complex. The influences of O_2 and a general protease inhibitor cocktail (Sigma Chemicals; catalog No. P2714) on "A" to "X" conversion were assessed by careful exclusion of O_2 in sample preparation and by adding 20 μL of a 0.1 g/L solution of the inhibitor cocktail in 4 h intervals to a split sample of *Nm*HO^A−PH−H_2O, where the second portion served as control.

NMR Spectroscopy. ^1H NMR data were collected on Bruker AVANCE 500 and 600 spectrometers operating at 500 and 600 MHz, respectively. Reference spectra were collected in both ^1H_2O and ^2H_2O over the temperature range 15−35 °C at a repetition rate of 1 s^{-1} using a standard one-pulse sequence. Chemical shifts are referenced to 2,2-dimethyl-2-silapentane-5-sulfonate (DSS) through the water resonance calibrated at each temperature. 600 MHz NOESY (*37*) spectra (mixing time, 40 ms; 15−35 °C) using both hard pulse and "3:9:19" detection (*38*) and 500 MHz Clean-TOCSY (to suppress ROESY response (*39*)) spectra (25°, 35 °C, spin lock 25 and 40 ms) using MLEV-17 (*40*) were recorded over a bandwidth of 25 kHz (NOESY) and 12 kHz (TOCSY) with recycle times of 500 ms and 1 s, using 512 t1 blocks of 256 scans each consisting of 2048 t2 points. 2D data sets were processed using Bruker XWIN software on a Silicon Graphics Indigo workstation and consisted of 30°- or 45°-sine-squared-bell-apodization in both dimensions, and zero-filling to 2048 × 2048 data points prior to Fourier transformation.

Simple molecular modeling of the C-terminus was carried out by the standard program in the Accelerys Insight package, using the X-ray coordinates (*21*) (PDB access 1J77) of residues 8−206 and the His207 peptide NH H-bond to the Asp27 carboxylate and the Arg208 guanidyl H-bond to the 7-propionate carboxylate as constraints.

Mass Spectrometry. Matrix assisted laser desorption ionization time-of-flight (MALDI-TOF) mass spectrometry was carried out on a Voyager DE system (Perseptive Biosystems) housed in the Washington State University Laboratory for Biotechnology and Bioanalysis, Unit 2 (WSU LBB2). Five primary matrix solutions were employed in replicates of each *Nm*HO sample. These were made from saturated solutions of sinapinic acid (3,5-dimethoxy-4-hydroxy-cinnamic acid, Aldrich or Sigma). The aqueous solutions used to dissolve the matrix were (i) 30%−0.1% trifluoroacetic acid/70% acetonitrile (Sigma) by volume; (ii) 30%−1.0% trifluoroacetic acid/70% acetonitrile; (iii) 50%−1.0% trifluoroacetic acid/50% acetonitrile; (iv) 30%−1.0% acetic acid/70% acetonitrile; (v) 50%−1.0%acetic acid/50% acetonitrile. Protein samples (1 μL) were thoroughly pipet mixed with an equal volume of the matrix solution on the MALDI-TOF plate until crystallization began. For calibration purposes, standard desalted solutions of (all from Sigma) equine myoglobin (M_r = 16 952.56) and equine cytochrome *c* (M_r = 12 361.14) were incorporated in some solutions as internal standards for accurate mass/charge determinations. Mass statistics were accumulated using repeated mass determinations in separate MALDI-TOF experiments with at least two internal references present. Individual protein masses were calculated using the averaged isotope masses of each element (IUPAC Commission on Atomic Weights and Isotopic Abundances, 1993): H = 1.007 94, C = 12.011, N = 14.006 74, O = 15.9994, S = 32.066. Protein masses were then constructed from the calculated mass of each amino acid and the specific primary amino acid sequence. The values reported are further rounded to units place.

N-Terminal Sequencing. Amino-terminal protein sequencing (up to 12 amino acids) was carried out in the Washington State University Laboratory for Biotechnology and Bioanalysis, Unit 1 (WSU LBB1), using an Applied Biosystems Procise 492 protein sequencer.

NmHO Activity. Optical absorption spectra were recorded on a Beckmann DU 7400 spectrophotometer at 30 °C between 250 and 750 nm. The standard reaction mixture consists of 10 μM *Nm*HO−PH−H_2O complex in 1.5 mL of 50 mM phosphate (pH 7.4). After 3 min preincubation, the reaction was started by the addition of 15 μL of 1 M sodium ascorbate (final concentration, 10 mM). When desferrioxamine was added, a final concentration of 1 mM was used.

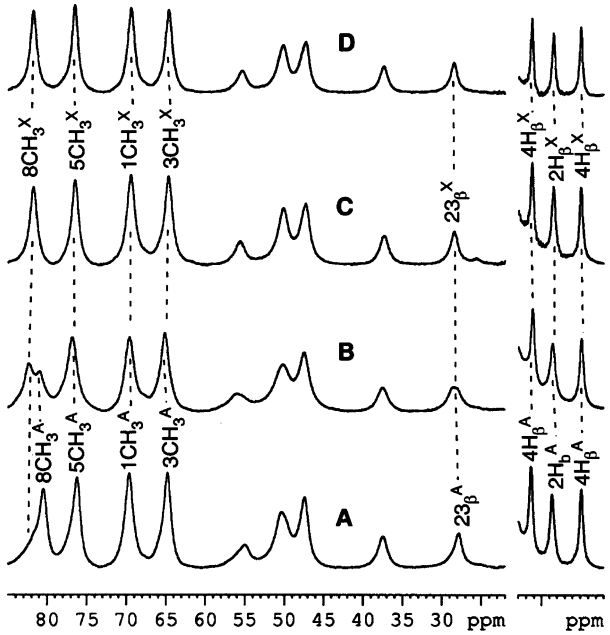

FIGURE 2: Resolved portions of the high-spin ferric *Nm*HO−PH−H_2O complexes in ^2H_2O, 100 mM in phospate, pH 7.0 at 25 °C as (A) the initially formed *Nm*HO^A−PH−H_2O complex with assigned methyl and vinyl H_β peaks; (B) a sample "aged" approximately 24 h at 25 °C that consists of ∼1:1 *Nm*HO^A−PH−H_2O:*Nm*HO^X−PH−H_2O; (C) a sample "aged" for a week at 25 °C which consists of predominantly *Nm*HO^X−PH−H_2O. (D) The NMR spectrum for the deletion mutant ΔC2-*Nm*HO−PH−H_2O (with Arg208His209 deleted) which is indistinguishable from the "aged" *Nm*HO^X−PH−H_2O complex in trace C.

Stereoselectivity of the reaction products was analyzed by HPLC (*41*) after being hydrolyzed with HCl to ensure the full conversion into biliverdin.

RESULTS

Effect of the "A" → "X" Conversion on NMR Spectra. The expected (*16*, *20*) and observed (*30*) dipolar contacts between protohemin and active site residues, and among active site residues, in WT *Nm*HO−PH−CN, are shown schematically in Figure 1. The unexpected contacts of His207 and Arg208 (each shown in bold) with pyrrole D observed (*30*) in *Nm*HO^A−PH−CN (and lost in *Nm*HO^X−PH−CN; see below) are shown by dashed lines. The resolved portions of the 500 MHz ^1H NMR spectrum of native or "A" high-spin *Nm*HO^A−PH−H_2O complex are illustrated in Figure 2A, where we provide the previously determined (*42*) heme methyl, vinyl H_β, and axial His $C_\beta H$ assignments. Figure 2B represents the ^1H NMR spectrum of a *Nm*HO−PH−H_2O sample "aged" ∼24 h at 25 °C that contains ∼45% *Nm*HO^A−PH−H_2O and ∼55% *Nm*HO^X−PH−H_2O, and Figure 2C represents the spectrum of a *Nm*HO−PH−H_2O sample aged for a week at 25 °C, which corresponds to >95% *Nm*HO^X−PH−H_2O. It is noted that in the high-spin, resting state complex reference NMR spectrum, only the $8CH_3$ "senses" the structural difference between the "A" and "X" complexes (in 2D NOESY, the *Nm*HO−PH−H_2O Asp24 C_βHs reveal altered chemical shifts, not shown; see Supporting Information). Moreover, some ∼10% of "X" is already present in the initial complex in Figure 2A, as shown by the low-field shoulder to the $8CH_3$ peak.

The resolved portions of the 600 MHz ^1H NMR spectrum of the wild-type enzyme as the *Nm*HO−PH−CN complex

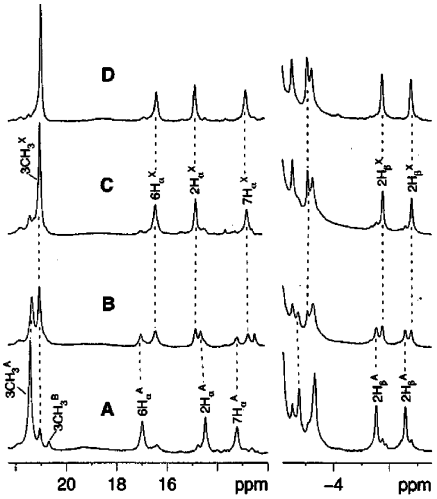

FIGURE 3: Resolved portions of the 600 MHz ^1H NMR spectra, in ^2H_2O, 50 mM phosphate, pH 7.0 at 25 °C, of (A) low-spin, predominantly *Nm*HO^A−PH−CN; (B) a ∼1:1 mixture of *Nm*HO^A−PH−CN and *Nm*HO^X−PH−CN (population achieved upon "aging" *Nm*HO−PH−H_2O for ∼40 h at 25 °C before adding CN^-), and (C) primarily *Nm*HO^X−PH−CN. Peaks are labeled by the Fischer notation for the heme (Figure 1), with the peaks for the alternate complexes, *Nm*HO^A−PH−CN and *Nm*HO^X−PH−CN, differentiated by a superscript A or X, respectively. (D) The ^1H NMR spectrum for the truncation mutant ΔC2-*Nm*HO−PH−CN, where Arg208His209 are deleted.

are displayed in Figure 3A. The major component (>90% and labeled species "A") represents the equilibrium, native complex, as also shown in Figure 2A (peaks with superscript A), with the PH orientation as described in both the crystal (*16*, *30*) and solution structures, and shown in Figure 1. The resonance assignments are those described in detail previously (*30*) for the PH orientation shown in Figure 1. Heme methyls for two minor components are also observed in Figure 3A. The peak labeled $3CH_3^B$ arises from the native *Nm*HO−PH−CN with PH rotated 180° about the α-γ-meso axis (species "B"). The "B" and "A" species are comparably populated immediately after assembling the complex in solution, but rapidly equilibrate to a 10:1 "A":"B" ratio (*30*), as shown in Figure 3A. A third (∼10%) species (*30*), which we designated "X", gives rise to methyl peak labeled $3CH_3^X$, is variably present upon preparing the complex under a variety of conditions, and corresponds to the species in Figure 3C. No further ^1H NMR changes are observed over several months after conversion to "X" as either the *Nm*HO^X−PH−H_2O or *Nm*HO^X−PH−CN complexes.

The "A" → "X" conversion in the *Nm*HO−PH−H_2O complex has a half-life of ∼24 h at 25 °C in the presence of ∼50 mM phosphate at pH 7.0. Interconversions among the "aged" *Nm*HO−PH−H_2O and *Nm*HO−PH−CN complexes reveals that the same species X is formed in the two derivatives (data not shown). The "A" → "X" half-life is significantly reduced by replacing the PH vinyls with methyls (Liu, Ma, Yoshida, La Mar, unpublished observations). Exclusion of O_2 from a sample had no detectable effect on the conversion rate for the *Nm*HO^A−PH−H_2O complex. Addition of cyanide slowed the "A" → "X" rate significantly for each hemin, but even the cyanide complex eventually converted to the "X" complex at a rate much faster upon replacing vinyls with methyls. Last, the introduction of a bacterial protease inhibitor cocktail failed to have a detectable effect on the rate of "A" → "X" conversion (NMR data

Table 1: Chemical Shifts for the Heme and Key Heme Pocket Residues for the "A" and "X" Forms of *Nm*HO−PH−CN

		*Nm*HO^X−PH−CN	*Nm*HO^A−PH−CN				*Nm*HO^X−PH−CN	*Nm*HO^A−PH−CN	
residue	proton	δ_{DSS}(obs)[a]	δ_{DSS}(obs)[b]	δ_{dip}(calcd)[c]	residue	proton	δ_{DSS}(obs)[a]	δ_{DSS}(obs)[b]	δ_{dip}(calcd)[c]
heme	1-CH_3	7.55	7.90		Val26	NH	8.31	8.33	1.89
	3-CH_3	21.00	21.40			$C_\alpha H$	2.79	2.80	−0.24
	5-CH_3	10.25	9.62			$C_\beta H$	1.62	1.60	1.23
	8-CH_3	10.77	10.33			$C_{\gamma 1}H_3$	−1.98	−1.96	−2.85
	2 vinyl	14.79, −5.77, −6.79	14.48, −5.58, −6.62			$C_{\gamma 2}H_3$	−0.52	−0.5	0.18
	4 vinyl	7.96, −3.09, −2.55	8.06, −3.38, −2.80		Leu119	NH	10.62	10.54	2.20
	6-C_αHs	1.26, 16.40	1.14, 16.92			$C_\alpha H$	4.71	4.72	1.40
	6-C_βHs	−0.88, −3.27	−1.02, −3.38			$C_{\beta 1}H$	−1.31	−1.15	−0.82
	7-C_αHs	12.62, 5.92	13.06, 5.73			$C_{\beta 2}H$	−1.20	−0.95	−0.13
	7-C_βHs	−1.23, −2.01	−1.10, −2.17			$C_\gamma H$	−0.48	−0.40	
	α-meso	−2.15	−2.21			$C_{\delta 1}H_3$	−1.71	−1.69	−0.30
	β-meso		8.13			$C_{\delta 2}H_3$	−0.70	−0.63	−2.54
	γ-meso	−1.64	−1.72		Gly120	NH	13.5	13.6	8.49
	δ-meso		6.43			$C_{\alpha 2}H$	5.72	5.75	3.45
Thr19	NH	8.11	8.04	0.61	Ala121	NH	15.23	15.32	9.63
	$C_\alpha H$	5.53	5.52	0.96		$C_\alpha H$	8.43	8.52	8.77
	$C_\beta H$	5.77	5.75	1.12		$C_\beta H_3$	5.51	5.44	5.06
	C_γH3	1.73	1.70	0.38	Phe123	NH	8.81	8.83	1.50
Thr20	NH	8.43	8.37	1.15		$C_\alpha H$	4.53	4.51	0.15
	$C_\alpha H$	6.41	6.30	3.19		$C_{\beta 1}H$	3.58	3.46	−0.54
	$C_\beta H$	5.17	5.14	1.22		$C_{\beta 2}H$	3.37	3.27	−0.59
	$C_\gamma H$	2.30	2.27	1.96		C_δHs	7.13	7.07	−0.81
Ala21	NH	9.37	9.36	1.37		C_ϵHs	7.02	6.94	−0.09
	$C_\alpha H$	5.35	5.31	1.56		$C_\zeta H$	7.19	7.15	−0.56
	$C_\beta H_3$	2.05	2.04	0.96	Phe181	C_δHs	7.22	7.25	0.16
His23	NH	11.17	11.08	3.44		C_ϵHs	7.68	7.72	0.40
	$C_\alpha H$	7.30	7.37	6.01		$C_\zeta H$	8.92	8.87	1.16
	$C_{\beta 1}H$	11.51	11.56		His *I* (207)	NH	?	9.15	−0.64
	$C_{\beta 2}H$	10.88	10.75			$C_\alpha H$	?	3.84	−1.22
	$N_\delta H$	16.37	16.36			$C_\beta H$	?	2.43	−0.54
	$C_\delta H$	18.4	19.2			$C_\beta H'$	?	2.22	−1.27
Asp24	NH	11.42	11.41	4.66		$C_\delta H$	7.08	6.59	0.12
	$C_\alpha H$	6.82	6.80	4.70		$C_\epsilon H$	7.93	7.68	0.22
	$C_{\beta 1}H$	3.76	3.67	2.02	Arg208	$C_\alpha H$	*d*	3.84	−0.48
	$C_{\beta 2}H$	4.30	4.30	2.37	His *J* (209)	$C_\delta H$	*d*	7.92	
						$C_\epsilon H$		6.99	

[a] Chemical shifts in ppm, referenced to DSS via the solvent signal, in ^1H_2O, 100 mM in phosphate, pH 7.0 at 25 °C. [b] Chemical shifts in ppm, referenced to DSS via the solvent signal, in ^1H_2O, 100 mM in phosphate, pH 7.0 at 25 °C, as reported by Liu et al. (*30*). [c] Calculated dipolar shift, in ppm, for *Nm*HO^A−PH−CN, as reported by Liu et al. (*30*). [d] Cleaved.

shown in Supporting Information). Hence copurified *Escherichia coli* proteases are not likely the cause of the "A" → "X" conversion. Clearly more extensive studies well outside the scope of this report are needed to elucidate this mechanism.

Structural Characterization of the Heme Cavity for NmHO^X−PH−CN. The hyperfine shift pattern for resolved resonances is very similar for *Nm*HO^A−PH−CN and *Nm*HO^X−PH−CN (compare Figures 3A and 3C), so that the same 2D ^{1}H NMR approaches reported in detail for the former complex (*30*) yield similarly complete assignments for the latter complex. Hence only very limited 2D data are provided that display *differences* in the two complexes. Additional 2D data for *Nm*HO^X−PH−CN are provided in the Supporting Information. The chemical shifts for the heme and the most strongly hyperfine-shifted residues in the two complexes are compared in Table 1, with the data for the remainder of the 55 assigned residues provided in the Supporting Information. Except for primarily the heme 8CH_3 and, more weakly, the heme 1CH_3 (see below), very similar NOESY cross-peak patterns between heme and residues, and among residues, are observed in the "A" and "X" *Nm*HO−PH−CN complexes.

The key differences in heme contacts between the "A" and "X" species are illustrated in the portions of the NOESY spectra involving the heme 8CH_3 and 1CH_3 peaks, as illustrated in Figure 4 for *Nm*HO^A−PH−CN (Figures 4A−4I) and *Nm*HO^X−PH−CN (Figures 4A′, 4H′, and 4I′), complexes. The crystal structures of *Nm*HO complexes predict (*16*, *21*) 8CH_3 NOESY cross-peaks only to Gly120 $C_\alpha H$ (under 7H_α in Figures 4A, 4B, but resolved at other temperatures). However, the actual NOESY spectra exhibit many more cross-peaks. For *Nm*HO^A−PH−CN (Figures 4A, 4B, 4C), a TOCSY-detected His ring (labeled His *I*), the C_βHs of the TOCSY-detected NH−$C_\alpha H$−$C_\beta H_2$ backbone of His *I* (His207) (Figure 4C), as well as the obvious $C_\alpha H$ of another residue exhibit significant intensity NOESY cross-peaks to the 8-CH_3. Since the $C_\alpha H$ peak at 3.84 ppm exhibits no common NOESY cross-peak to the rings of either His207 or His209 (see below), it can be assigned to the only other possible residue, Arg208. One of the His *I* C_βHs exhibits a weak cross-peak to the heme 1CH_3 (Figure 4D). It is noted that the peptide NH for His *I* (207) (Figure 4C) resonates well to the low-field of the overwhelming majority of the residues, indicating that it participates in a relatively strong H-bond (*29*, *30*, *33*, *43*, *44*).

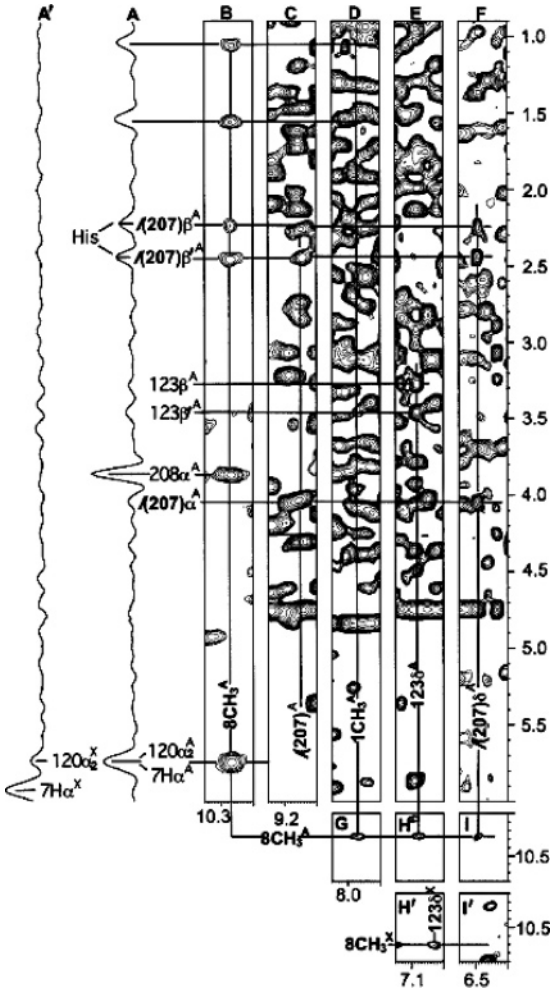

FIGURE 4: Portion of the 600 MHz ^{1}H NOESY spectrum (B−I, H′, I′) and NOESY slices through diagonal (A, A′) (mixing time 40 ms, repetition rate 1 s^{-1}); in ^1H_2O, 100 mM in phosphate, pH 7.0 at 25 °C, of *Nm*HO^A−PH−CN (A−I) illustrating $8CH_3$ NOESY cross-peak to His *I* (207) C_βHs and Arg208 C_αH (A, B), His *I* (207) C_δH (F), and Phe123 ring (H), $1CH_3$ NOESY cross-peak to His *I* (207) C_βH (D), and His *I* (207) intrabackbone connection (C); and of *Nm*HO^X−PH−CN illustrating lack of either His *I* (207) or Arg208 C_αH cross-peak to $8CH_3$ (A′), and His *I* (207) ring cross-peak to 8-CH_3 (I′), but the retention of the Phe123 ring cross-peak to 8-CH_3 (H′). The loss of the His *I* (207) and Arg208 cross-peaks is particularly clear in the comparison of the slices through the $8CH_3$ for the two complexes (A, A′).

With a confirmed conserved molecular structure for residues Phe11−Phe192 for *Nm*HO^A−PH−CN in solution (*30*) relative to that in crystal structures (*20*, *21*), this His *I* has been concluded to arise from the C-terminal fragment His207-Arg208-His209 found "missing" in the crystal structures. The $8CH_3$ cross-peaks to the ring of Phe123 (Figure 4H) are stronger than predicted by the crystal structure, but can be accounted for by a small rotation of the Phe123 side chain, as discussed previously (*30*). Comparison to the same spectral window for the $8CH_3$ peak of *Nm*HO^X−PH−CN demonstrates (particularly clearly observed in the NOESY $8CH_3$ slices, Figures 4A and 4A′) that both the His *I* ring and its backbone (not shown) NOESY cross-peaks are completely lost, with only the $8CH_3$/Phe123 ring contact remaining (Figure 4H′). Several other cross-peaks to $8CH_3$ in the upfield aliphatic window (Figures 4A, 4B), which for *Nm*HO^A−PH−CN have been attributed to Arg208 side chain protons, are similarly absent in the "X" complex (Figure 4A′).

The heme hyperfine shifts of the low-spin CN^- complex are perturbed by the "A" → "X" conversion (Table 1), but not in any pattern consistent with rotation of either the heme or axial His (*35*). Rather, the perturbation appears to manifest itself more in the pyrrole C/D portion of the heme. The local nature of the perturbation in the "A" → "X" conversion is dramatically evidenced in the high-spin complex (compare Figures 2A and 2C), where only the $8CH_3$ peak exhibits a detectably different environment in the two species. (All other resolved resonances exhibit essentially identical shifts in the "A" and "X" complexes). The dipolar shifted residues in both *Nm*HO−PH−CN and *Nm*HO−PH−H_2O, with the exception of the distal Leu119 and the proximal Asp24 in the former, and Asp24 in the latter (see below), exhibit essentially indistinguishable shifts and NOESY cross-peak patterns in the "A" and "X" complexes (Table 1), indicating a highly conserved structure of the heme pocket, except at the solvent exposed pyrrole D.

Thus the most dramatic structural differences between the "A" and "X" *Nm*HO−PH−CN species is the *complete loss of the $8CH_3$ interaction with the C-terminal residue* His *I* (207)/Arg208 in the "A" → "X" conversion. The loss of this interaction with the C-terminus is the source of the sole perturbation of the $8CH_3$ chemical shift in the high-spin complex "A" → "X" conversion (Figures 2A−2C).

C-Terminal Cleavage in NmHO^X. Identical mass spectra were detected for *Nm*HO^A whether the apo or substrate complexes were employed (not shown), confirming denaturation of the complex in the matrix. The predicted molecular mass of Met1−His209 *Nm*HO is 23 590 Da. The [*Nm*HO^A + H]$^{+1}$ ([*Nm*HO^A + 2H]$^{+2}$) peak in the MALDI-TOF mass spectrum of "native" or *Nm*HO^A is observed at 23 454 ± 13 (11 728 ± 5) Da (Figure 5A), using horse apo-Mb (M_r 16 952) as internal standard, which reflects a 135 ± 13 Da difference (mass reduction) of neutral *Nm*HO^A relative to that calculated for neutral Met1−His209. This difference is equally consistent with a missing Met1 (M_r 131 Da) or His209 (M_r 137 Da). N-Terminal sequencing of *Nm*HO^A reveals a homogeneous Ser-Glu-Thr-Glu-Asp-Glu-Leu-Thr-Phe, which uniquely identifies Ser2−Phe11 of the *Nm*HO sequence and demonstrates that Met1 is cleaved during the processing of the enzyme in *E. coli*. Hence the isolated enzyme (species "A" or *Nm*HO^A) unequivocally consists of Ser2−His209 (with calculated neutral M_r = 23 459 Da).

Mass spectrometry of ∼10:1 and ∼1:10 mixtures of *Nm*HO^A and *Nm*HO^X (as determined by ^{1}H NMR in the cyanide complex) reveals a decreasing intensity for the peak centered at 23 454 ± 13 Da (labeled [*Nm*HO^A + H]$^+$) as shown in Figures 5B and 5C, respectively, which reflects a mass indistinguishable from that identified for pure *Nm*HO^A in Figure 5A, and a new peak labeled [*Nm*HO^X + H]$^{+1}$, with *m*/*z* 23 166 ± 6 Da, which reflects a reduction of neutral molecular mass relative to that calculated for Ser2−His209 *Nm*HO^A by 288 ± 13 Da. N-Terminal sequencing of the "A":"X" mixture again indicates a dominant (>90%) component with sequence identical to that obtained for pure *Nm*HO^A, dictating that the mass reduction in "X" relative to "A" *occurs at the C-terminus*. The calculated M_r for Ser2−Pro206, Ser2−His207, and Ser2−Arg208 is 23 028, 23 166, and 23 322 Da, respectively. Only the mass of Ser2−His207,

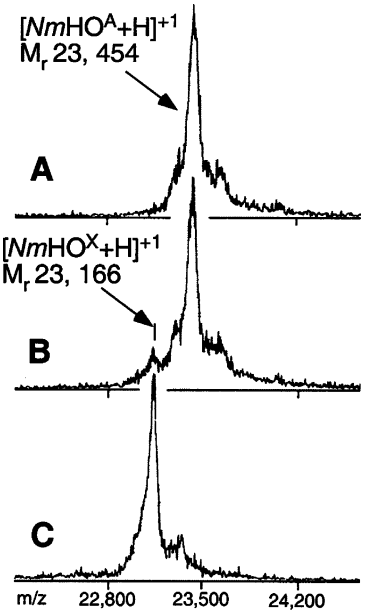

FIGURE 5: Portion of the MALDI-TOF mass spectra for M_r^+, obtained on the matrix consisting of sinapinic acid. Equine apoMb (calcd $M_r = 16\,952$) was used as internal calibrant. (A) Essentially pure (>95%) *Nm*HO^A, which gives rise to $[NmHO^A + H]^{+1} = 23\,454 \pm 13$ Da, and $[NmHO^A + 2H]^{+2} = 11\,728 \pm 5$ Da (not shown), indicative of a polypeptide 135 ± 15 Da smaller than that calculated for the sequence Met1−His209 ($M_r = 23\,590$), but consistent with *Nm*HO^A as Ser2−His209. (B) A ~10:1 *Nm*HO^A:*Nm*HO^X mixture, which yields a $[NmHO^A + H]^{+1}$ peak of $23\,454 \pm 13$ and a weak new peak with $M_r = 23\,166 \pm 10$ assigned to *Nm*HO^X. (C) A ~1:10 *Nm*HO^A:*Nm*HO^X mixture (as determined by NMR) shows the new peak in B, as now the major peak at $23\,166 \pm 10$, and only a weak *Nm*HO^A peak at $23\,459 \pm 15$ Da. It is clear that the new peak with M_r ~23 166 Da represents the "aged" *Nm*HO^X that corresponds to Ser2−His207 with Arg208His209 cleaved.

23 166 Da, is consistent with the observed value of 23 166 ± 6 Da (neutral mass), dictating that the species "X", or *Nm*HO^X, corresponds to Ser2−His207, which is equivalent to WT or species "A" with Arg208 and His209 deleted. Only the $23\,454 \pm 13$ and $23\,166 \pm 6$ Da peaks are detected at intermediate degrees of A → X conversion (not shown), suggesting that the Arg208His209 is cleaved as a dipeptide.

Assignment of His Rings. Long mixing time (40 ms) TOCSY spectra for primarily the *Nm*HO^A−PH−CN complex in ^2H_2O reveal the cross-peaks between the ring $C_\delta H$ and $C_\epsilon H$ for 10 His, (not shown; see Supporting Information). With previous identification (*30*) of the strongly relaxed axial His23 ring (*30*), this locates all eleven of the His rings in native *Nm*HO^A. Previous 2D NOESY contacts to the C_δHs, together with the conserved molecular structure for residues Phe11−Phe192 in solution relative to that in the crystal, had definitively identified (*30*) eight of the His rings (His23, 53, 58, 127, 137, 141, 145, 152; chemical shifts provided in the Supporting Information (*30*). The three remaining TOCSY ring cross-peaks, with chemical shifts included in Table 1 (His *I* and *J*) and the Supporting Information (His *K*), are labeled His *I* (close to 8-CH_3 in "A" complex), His *J*, and His *K* (which collectively must arise from His159, 207, and 209); none of these three His rings exhibit any NOESY cross-peaks that aid in their assignment.

Conversion of "A" → "X" results in a TOCSY spectrum that also detects 10 rings (not shown; see Supporting Information). Seven His rings (plus the axial His23) exhibit the same diagnostic NOESY cross-peaks that allow their assignments as reported for the "A" complex (*30*) (not shown); the ring proton chemical shifts for these seven His rings are essentially independent of the "A" → "X" conversion (see Supporting Information). The TOCSY cross-peak for His *I* of the "A" species is clearly lost (as in its TOCSY-detected His *I* $NHC_\alpha HC_\beta H_2$ backbone; not shown) in the "X" species. Neither His *M* nor His *N* in *Nm*HO^X−PH−CN (Table 1), that collectively must arise from His159 and His209, exhibits any detectable NOESY cross-peak to the ring to guide their identification. Based on the observation that the ring shifts for the other seven assigned His are completely conserved in "A" and "X", the same shifts for His *K* in "A" and His *M* in "X" argue for their assignment to His159, which is relatively remote from both C-terminus and heme. Hence His *N* in "X" must arise from His207, and its lack of NOESY cross-peak argues for an orientation toward the solvent, as is consistent with its shifts. Formation of "X" is also accompanied by the appearance of a new His ring peak at 8.30/6.78 ppm. Ultrafiltration of the solution reduces the intensity of peaks for this His *N* ring, supporting the origin of this ring as the cleaved His209. The absence of additional NOESY cross-peaks does not allow the determination by 2D ^{1}H NMR alone whether His207 or His209 interacts with the heme 8CH_3 in *Nm*HO^A−PH−CN. Modeling the C-terminal interaction with the heme, however, strongly favors assignment of His *I* (in contact with 8CH_3) as His207 (see below).

Nonetheless, the His ring TOCSY spectra provide additional evidence for the loss of a His ring in the "A" → "X" conversion, and the combination of the NMR, mass spectrometry, and N-terminal sequencing data clearly demonstrates that "aging" native *Nm*HO leads to loss of the two C-terminal residues, Arg208His209, and the abolition of the C-terminus interaction with the substrate.

Cyanide Affinity in NmHO^A and NmHO^X. Our interest here is to determine the ratio of their cyanide binding constants. With $K^i_{eq} = [NmHO^i{-}PH{-}CN]/[CN^-][NmHO^i{-}PH]$ for i = "A" or "X", we obtain

$$K^A_{eq}/K^X_{eq} = [NmHO^A{-}PH{-}CN][NmHO^X{-}PH]/[NmHO^X{-}PH{-}CN][NmHO^A{-}PH] \quad (1)$$

The two ratios, $[NmHO^A{-}PH{-}CN]/[NmHO^X{-}PH{-}CN$ and $[NmHO^X{-}PH]/NmHO^A{-}PH]$, in eq 1 are determined from the relative intensities of the heme methyl peaks for the low-spin (Figures 6A′−6F′) and high-spin (Figures 6A−6F) complexes under conditions where both the "A" and "X" complexes are significantly populated. As shown in Figure 6, the high-spin species 8CH_3^A peak preferentially loses intensity upon CN^- addition (Figures 6A−6F), while the low-spin species 3CH_3^A peak preferentially gains intensity relative to 3CH_3^X (Figures 6A′−6F′), dictating a stronger CN^- binding in the "A" than "X" species. The quantitation of the intensities by simulation yields $K^A_{eq}/K^X_{eq} = 1.7 \pm 0.2$.

NMR Spectra for the des-Arg208His209 Deletion Mutant ΔC2-NmHO. The resolved portions of the ΔC2-*Nm*HO−H_2O and ΔC2-*Nm*HO−PH−CN ^{1}H NMR spectra are provided in Figures 2D and 3D, respectively. Comparison of these to the analogous *Nm*HO^X−PH−H_2O and *Nm*HO^X−

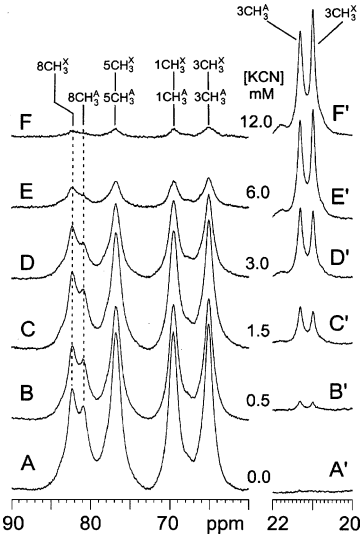

FIGURE 6: Low-field portion of the ^{1}H NMR spectra of: (A−F) the high-spin *Nm*HO−PH−H_2O and (A′−F′) low-spin *Nm*HO−PH−CN complexes for a 45:55 mixture of *Nm*HO^A−PH:*Nm*HO^X−PH, ∼3 mM in *Nm*HO, as a function of [CN^-], in mM. Note preferential loss of 8CH$_3^A$ relative to 8CH$_3^X$ intensity upon increasing [CN^-] for the high-spin complex A → F, and preferential increase of 3CH$_3^A$ relative to 3CH$_3^X$ intensity of low-spin complexes in A′ → F′.

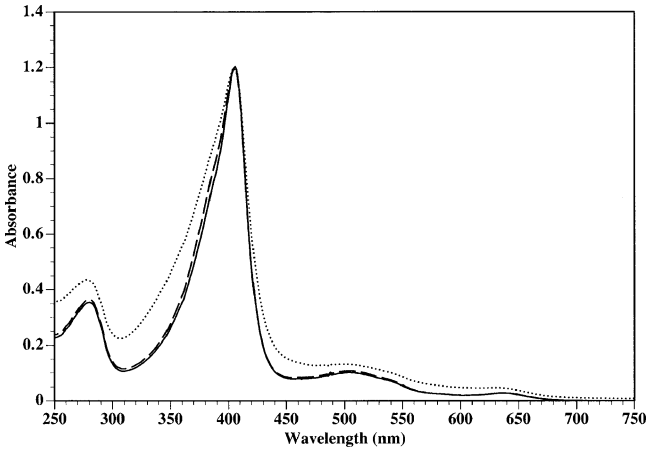

FIGURE 7: Absorption spectra of the *Nm*HO−PH−H_2O complexes. Solid line, 10 mM of WT *Nm*HO−PH−H_2O complex; dotted line, about 10 mM of *Nm*HO^X−PH−H_2O (an appropriate amount of the "X" species was used so that the intensity of the Soret band is equal to that of wild-type complex); dashed line, 10 mM of ΔC2-*Nm*HO−PH−H_2O.

PH−CN spectra in Figures 2C and 3C, respectively, reveals them to be indistinguishable in both the high-spin and low-spin complexes. This confirms not only that Arg208His209 are cleaved in the "aged" *Nm*HO^X but that this is the only perturbation in the "aging". 2D NOESY spectra similarly reveal indistinguishable shifts and dipolar connectivities in the low-spin derivative (not shown).

Heme Degradation Bound to NmHOs with Ascorbate. The UV−visible spectra of the PH complexes of WT *Nm*HO−PH−H_2O and the mutant ΔC2-*Nm*HO−PH closely resemble each other (Figure 7). *Nm*HO^X−PH−H_2O exhibited some differences from those of the above two enzymes, in that the ratio of the absorption at 406 nm to 280 nm (2.8) was slightly smaller than that (3.3) of the heme complex of wild-type enzyme. This suggests that the either "X" species used in the present study included a little apo-enzyme resulting from release of a little heme during the conversion of the "A" species to the "X" species or some aggregation causes light scattering.

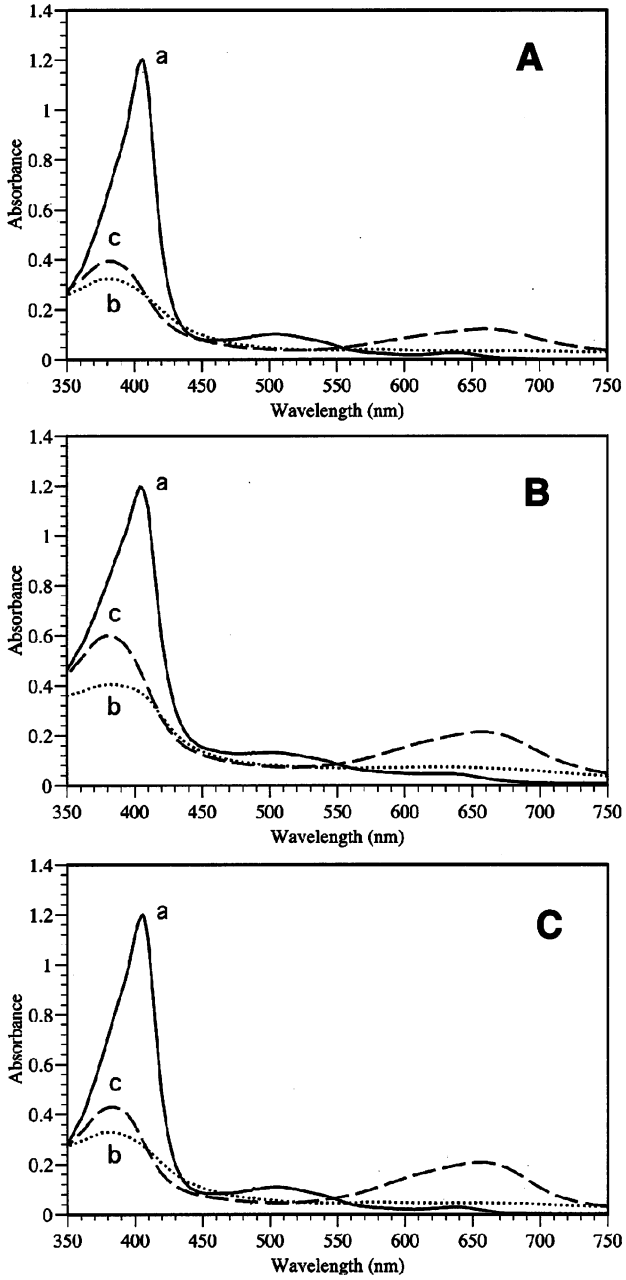

FIGURE 8: Ascorbate-driven degradation of PH bound to *Nm*HOs in the absence or presence of desferrioxamine. Reaction mixture contained 10 mM *Nm*HOs in 1.5 mL of 50 mM KPB (pH 7.4). After 3 min preincubation, the reaction was started by the addition of 15 mL of 1 M sodium ascorbate (final concentration, 10 mM). When desferrioxamine was added, a final concentration of 1 mM was used. (A) WT *Nm*HO^A; (B) the *Nm*HO^X species; (C) ΔC2-*Nm*HO. Spectrum a (solid line), before the start of the reaction; spectrum b (dotted line), 25 min after the start of the reaction without desferrioxamine; spectrum c (dashed line) 25 min after the start of the reaction with desferrioxamine.

The ascorbate-driven activity resulting in degradation of PH was monitored by UV−visible spectroscopy for the three complexes, WT *Nm*HO−PH−H_2O, *Nm*HO^X−PH−H_2O, and ΔC2-*Nm*HO−PH−H_2O. The WT *Nm*HO−PH−H_2O complex (Figure 8A, spectrum a) was quantitatively converted to ferric biliverdin (spectrum b), as previously reported (*45*). Yoshida and Kikuchi (*46*) found that rat HO-1 in the presence

of ascorbate yields ferric biliverdin, which yields the iron-free biliverdin on the addition of desferrioxamine, a ferric ion chelator. Therefore, we conducted a similar experiment in the presence of desferrioxamine. The heme degradation rate was not affected by desferrioxamine, but a spectrum recorded 25 min after the start of the reaction showed a new broad absorption in the red region (spectrum c), suggesting a partial conversion of ferric biliverdin to iron-free biliverdin.

Figure 8B shows that the spectral changes observed for the *Nm*HO^{X}−PH−H_2O complex with ascorbate. When incubated with ascorbate alone, PH of this speices was degraded at a rate, and with resulting spectrum, very similar to those of wild-type enzyme, indicating that the final product is ferric biliverdin. However, when the reaction with *Nm*HO^{X}−PH−H_2O was conducted in the presence of desferrioxamin, the intensity of the broad band observed in the red region after 25 min incubation increased intensity by a factor ~2 (spectrum c in Figure 8B) as compared to that for the WT complex wild-type enzyme. As shown in Figure 8C, the reactivities of ΔC2-*Nm*HO−PH−H_2O complex are essentially the same as those of the *Nm*HO^{X}−PH−H_2O species. The product biliverdin revealed exclusively α-stereoselectivity (data not shown) for both *Nm*HO^{X} and ΔC2-*Nm*HO, as reported for WT *Nm*HO.

These results indicate that, while neither the rate of heme degradation nor the stereoselectivity are detectably perturbed upon truncating *Nm*HO at the C-terminal by two residues, the truncation does influence the facility with which the product ferric biliverdin is released from the enzyme.

DISCUSSION

The Nature of the NmHO "Aging". The available NMR and mass spectrometry data on the in situ "aged" WT *Nm*HO and the NMR data on the synthetic ΔC2-*Nm*HO mutant, where Arg208 and His209 are deleted, clearly show that the "spontaneous aging" of *Nm*HO results in the cleavage of the two C-terminal residues that interact with the substrate pyrrole D in the WT *Nm*HO−PH−CN complex. While the mechanism of this aging is not understood at this time, it does not appear to be the result of either simple oxidative damage or the action of adventitious proteases which could copurify with *Nm*HO, and requires additional work well outside the scope of this report. What is important is that this "aging" of the resting state complex is sufficiently rapid to potentially interfere with all spectroscopic and functional studies carried out over a period of more than a few hours. The available new NMR results allow us to propose an improved model for the C-terminal interaction with substrate in the WT *Nm*HO−PH−H_2O complex that can account for altered functional properties of the "aged" complex.

Structural Changes Accompanying the C-Terminal Cleavage. The essentially indistinguishable 2D NOESY maps for *Nm*HO^{X}−PH−CN and the mutant ΔC2-*Nm*HO−PH−CN indicate that *Nm*HO^{X} and ΔC2-*Nm*HO are identical, and that our structural conclusions derived in detail for *Nm*HO^{X}−PH−CN are equally valid for the truncation mutant. The sequence origin of His *I*, in contact with the $8CH_3$, is either His207 or 209, but its identity could not be established on the basis of the presently available NOESY contacts alone. However, the available constraints do allow some limited modeling of the C-terminal His207Arg208His209 fragment that argues strongly for His *I* being His 207. In addition to the obvious loss of the His207 and Arg208 interaction with pyrrole D of the substrate, the deletions result only in very minor chemical shift change for the remainder of the active site. The heme resonances of the low-spin *Nm*HO−PH−CN complex exhibit some perturbation of chemical shifts in the "A" → "X" conversion, but the pattern of shifts, large spin density at heme positions 2, 3, 6, and 7, and smaller spin density at positions 1, 4, 5, and 8, reflective of the orientation of the axial His relative to the heme, is conserved (*35*). In general, the substituents on pyrrole C and D exhibit the largest fractional change in hyperfine shifts. The majority of the dipolar shifted residues in the active site display insignificant shift changes with the loss of the C-terminus (Table 1 and Supporting Information). Particularly noteworthy are the completely conserved dipolar shifts for the proximal residues Thr19−Val26 (with one exception, Asp24; see below) and key distal residues Cys113−Phe123 (with the exception of Leu119; see below), which dictate completely conserved magnetic axes in the "A" and "X" complexes. The two residues with the largest shift perturbations, the proximal side Asp24 and distal Leu119 (Table 1), are rationalized by their very close proximity to the heme contact with the C-terminus in the *Nm*HO^{A}−PH−CN complexes (see below).

For the high-spin *Nm*HO−PH−H_2O "A" and "X" complexes, only the $8CH_3$ of the resolved resonances exhibits detectably different hyperfine shifts for the heme (Figure 3A and Supporting Information), consistent with the primary contact of the C-terminus with $8CH_3$. The only assigned protons that exhibit (*42*) detectable shift change in the "A" → "X" transition in the high-spin complex are the proximal Asp24 C_βHs ($C_{\beta 1}$H 0.1 ppm difference between "A" and "X" complexes; see Supporting Information). 2D ^{1}H NMR NOESY maps of apo*Nm*HO^{A} and apoNmHO^{X} (not shown) are indistinguishable upon cursory inspection. The detectable difference in ^{1}H hyperfine shift pattern of the "A" and "X" PH complexes in the low-spin cyanide-inhibited forms shows that this is the optimal derivative for detection and structural characterization. However, at this stage, the most readily accessible technique for identifying the presence of *Nm*HO^{X} in any preparation, even in very small samples, is mass spectrometry.

A Model for WT NmHO Species "A". There are insufficient NMR data available, and likely inaccessible by solely ^{1}H NMR, to construct a quantitative molecular model for the C-terminus interaction with the heme pocket for the *Nm*HO^{A}−PH−CN complex. Such a study would require minimally ^{15}N, and likely both ^{15}N and ^{13}C, labeling of *Nm*HO, and 3D NMR, and is well beyond the scope of the present report. The route to efficient isotope labeling of *Nm*HO is under study. However, the presently determined data do provide sufficient constraints to generate a qualitative model that accounts for the present observations, suggests consequences for functional roles for this interaction, and provides a potential rationalization for the "loss" of the C-terminus in the crystal structures (*20*, *21*). The most important of the new NMR data is the location of the complete backbone of His 207 which interacts strongly with the $8CH_3$ (and weakly with $1CH_3$) and the recent report on the high-spin *Nm*HO^{A}−PH−H_2O complex where the resolved Asp24 C_βHs to Pro206 NOESY cross-peak predicted

by the crystal structure could be detected (*42*). The expected NOESY cross-peaks between the assigned Asp24 C_βHs and Pro206 in the low-spin *Nm*HO−PH−CN complex are completely lost in the very intense aliphatic region of the NOESY map (*30*). Thus the position of Pro206 in the crystal structure appears conserved in solution for *Nm*HO−PH complexes.

Our qualitative model results from the following data and their implications. First, we note that the ring protons for resonances His *I* and *J* (collectively His207 and 209) exhibit only very weak temperature-dependent chemical shifts, indicative of very small δ_{dip}, which argues for both ring orientations directed away from, rather than toward, the heme. Hence, imidazole ring contacts to the heme pocket are very unlikely candidates for the interactions that stablize the C-terminus contact with the heme pocket. This necessarily leaves the Arg208 guanidyl group as the main "anchor" to the heme pocket. Moreover, if the Pro206 position in the crystal is largely maintained in solution, His207 is restricted to heme pocket interactions solely on the *proximal side*, with Arg208 restricted to either peripheral or distal interactions with the heme pocket. An orientation of the Arg208 side chain toward the heme dictates an "outward" orientation of the ring of His209.

The following NMR data argue for the His *I* peptide NH as serving as a robust H-bond donor to a strong H-bond acceptor in order to orient the C-terminus: (a) moderate intensity NOESY (Figure 4A, 4B) cross-peak between significantly upfield dipolar shifted C_βHs (by variable temperature behavior) of His *I* and PH 8CH_3 (a weak His *I* C_δH−8CH_3 NOESY cross-peak likely arises via a secondary effect 8CH_3−C_βH−C_δH); (b) only a very low intensity NOESY cross-peak between the His *I* C_βHs and PH 1CH_3 (Figure 4D); (c) a substantial low-field bias for the His *I* peptide NH (Figure 4C) when compared to the majority of the other NHs in the complex, in spite of a predicted upfield dipolar shift for protons in this region of space (Table 1); and (d) His *I* (207) NH exhibits only moderate intensity loss upon saturating the solvent signal (not shown), indicating a very slow exchange rate for pH 7.0 indicative of significant dynamic stability (*33*, *47*, *48*) for the interaction between the C-terminus and the substrate.

The only realistic acceptor for the Arg208 guanidyl terminus is the carboxylate of the 7-propionate on PH. For the His207 peptide NH, the only "free" strong acceptor is the Asp27 carboxylate side chain. Using the constraints of a strong Arg208 guanidyl-7-propionate carboxylate salt bridge and a His207 peptide NH to Asp27 carboxylate H-bond, and moderate distance (∼4 Å) between 8CH_3 and both His207 C_βHs and Arg208 C_αH (based on NOESY cross-peaks), molecular dynamics and energy minimization with conserved geometry of Phe11−Pro206 resulted in a qualitative model consistent with the proposed constraints, albeit not at the ideal distances. Releasing the Pro206 restriction leads to insignificant movement of this residue (∼0.5 Å), but yielded "good" His207 peptide H-bond and Arg208 salt bridge distances of ∼3 Å. A molecular model for this C-terminus interaction with the active site in *Nm*HO^A−PH−CN is displayed in Figure 9. No unique orientation for the His209 ring is obtained, but it is shown oriented away from the heme pocket, as predicted above. The cleavage of Arg208His209 to form *Nm*HO^X abolishes the major stabilizing interaction

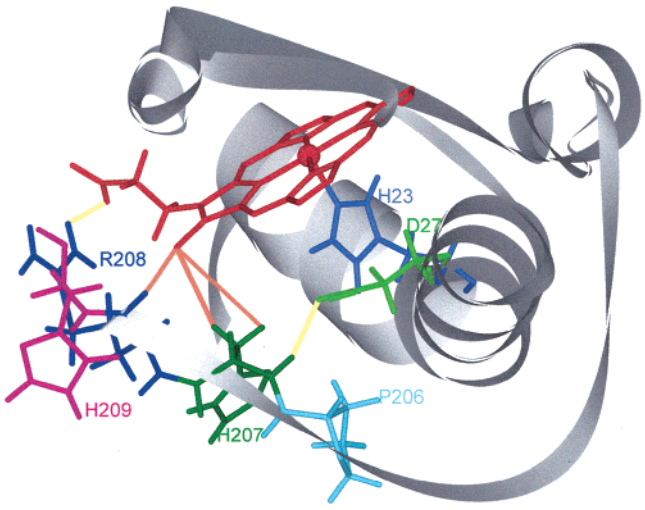

FIGURE 9: Molecular model of the C-terminus of *Nm*HO^A−PH−CN with His207 (dark green) making a H-bond (yellow line) with the carboxylate of Asp27 (light green), and the guanidyl group of Arg208 (dark blue) making a salt-bridge (yellow line) with the carboxylate of the 7-propionate of PH (red). The crystallographic detected Pro206, the penultimate His209, and the axial His25 are shown as light blue, magenta, and dark blue, respectively. Orange lines reflect important NOESY contacts of the PH 8-CH_3 with the Arg208 C_αH and the two His207 C_βHs.

between the C-terminus and heme, the Arg208-7-propionate link. The predicted dipolar shifts for His209 are included in Table 1 and are qualitatively consistent with the temperature dependence of the C_βH chemical shifts.

The side chain perturbation of the Asp24 C_βH shifts in both the high-spin (see Supporting Information) and low-spin complexes (Table 1) during the "A" → "X" conversion is consistent with the loss of the His207 peptide NH H-bond to a proximal helix carboxylate. The carboxylate of both Asp24 and Asp27 on the proximal helix are sufficiently close so as to expect a significant chemical shift perturbation of one of the side chain protons if a salt bridge is broken in the adjacent carboxylate. The Asp27 residue signals have not been assigned in the low-spin complex (they are under the intense aliphatic envelope)(*30*) and are too strongly relaxed to resolve in the high-spin complex (*42*). It is noted that in other HOs (*16*, *18*, *22*) the carboxylate of the homologue to Asp27 serves as H-bond acceptor to the axial His ring N_δH. However, in *Nm*HO, the H-bond to the axial His is provided by Asp24 (*16*, *21*), freeing Asp27 to interact with the C-terminus. The perturbation of the Leu119 shifts in the low-spin complex (Table 1) can be expected in the "A" → "X" conversion because the Leu119 interacts strongly with the 7-propionate whose H-bond with Arg208 is broken.

Implications for Function and Crystal Structures. The demonstrated contact between the C-terminus and the substrate argues for some functional role for this interaction. On the one hand, the loss of the C-terminal contact with the heme in the "X" form leads to a modest factor 1.7 ± 0.2 decrease in cyanide affinity. The structural comparison and conserved dipolar shifts of the "A" and "X" forms reveal that the orientation of the magnetic axes is quantitatively conserved in the "A" → "X" conversion, arguing against direct contact between the C-terminus and ligand. However, compensation of the negative 7-propionate carboxylate charge in the distal pocket by the positive Arg208 guanidyl

group in the native complex would be expected to facilitate the binding of negative ions in the "A" forms.

The specifics of heme degradation in either *Nm*HO^X−PH−H_2O or the mutant ΔC2-*Nm*HO−PH−H_2O complexes are unchanged from those in the WT *Nm*HO^A−PH−H_2O and maintain the unique α-stereoselectivity. Thus the C-terminal interaction does not appear to serve a role in the factors that stabilizes the ferric hydroperoxy intermediate or direct it toward the α-meso position by sterically orienting the hydroperoxy ion and blocking the other three meso positions. Moreover, essentially the same ferric biliverdin complexes are found in the truncated derivative and WT. What is notable is the significantly increased formation of free α-biliverdin in the presence of desferrioxamine upon deletion of the C-terminal Arg208His209 as either *Nm*HO^X or ΔC2-*Nm*HO. Thus the C-terminal interactions appear to retard loss of product.

The product biliverdin of the HO reaction is generally toxic, and the overall HO rate is very slow (∼0.03 s^{-1}) for all HOs (*9*). In mammals, the biliverdin off-rate is enhanced ∼50-fold upon binding biliverdin reductase, BVR, in a transient 1:1 complex, where the "docking" site has been identified (*14*) as the region of HO with the solvent exposed pyrrole. The enzyme that further processes biliverdin in pathogenic bacteria has not yet been identified. The effect on the product biliverdin off-rate upon eliminating the C-terminus suggests that the partner enzyme that processes the α-biliverdin may "extract" the C-terminus of *Nm*HO upon "docking", thereby facilitating product release. A more quantitative description of the detailed interaction of the C-terminus with substrate is clearly necessary, and routes to isotope labeling and structural characterization of the NMR-addressable *Nm*HO−PH−CN complex are in progress. However, preliminary data on the native *Nm*HO cyanide-inhibited substrate complex indicate that the C-terminal interaction with substrate can be significantly modulated by modifying the pyrrole substituents on pyrrole A and/or B (Liu, Y., Ma, L., Zhang, X., Yoshida, T., Satterlee, J. D., La Mar, G. N., unpublished). Since conversion of PH to its intermediates, α-hydroxy-PH, α-verdoheme, and ferric-α-biliverdin modifies the heme periphery near the pyrrole A/B junction, it is likely that the C-terminal interaction will depend on the nature of the intermediate, and structural characterization of the PH complex may or may not be relevant to the interaction of *Nm*HO-bound ferric-α-biliverdin.

Last, the relative ease with which the "A" → "X" "aging" takes place in the laboratory in the absence of strong field ligands for the substrate complexes suggests the possibility that properties of *Nm*HO have been measured and reported on samples that may contain a significant amount of the "X" form. The findings that the C-terminal His207Arg208His209 are "missing", and attributed to disorder in the crystal structure (*20*, *21*), could also be interpreted by a structure that has a significant fraction of the "X" form with the Arg208His209 cleaved and His207 oriented randomly toward the solvent. Mass spectral data on the *Nm*HO samples used for the crystal structure would resolve this issue.

CONCLUSIONS

Solution ^{1}H NMR spectroscopy and mass spectrometry show that the heme oxygenase from *N. meningitidis* spontaneously cleaves its two C-terminal residues, Arg208His209. Two of the three C-terminal residues, His207Arg208, interact with the substrate in the native enzyme in a manner that appears to stabilize the bound form of the product ferric-α-biliverdin. The cleavage occurs over a wide range of rates depending on the nature of the substrate and axial ligand and is not inhibited in the absence of O_2 or in the presence of protease inhibitor cocktail. The spontaneous reaction is sufficiently facile in the resting state substrate complex (half-life ∼24 h at 25 °C, pH 7.0) to require great care in physicochemical characterization of *Nm*HO complexes that may be variably, to completely, converted into the "aged" derivative. The reported "loss" of the C-terminal fragment in the crystal structure may have its origin in degraded HO. Comparison of the "aged" HO with the mutant with the two C-terminal residues deleted indicates that the C-terminal cleavage is the only process involved in the "aging".

SUPPORTING INFORMATION AVAILABLE

Five figures (upfield NOESY spectra of *Nm*HO^A−PH−H_2O/*Nm*HO^X−PH−H_2O; ^{1}H NMR of *Nm*HO^A−PH−H_2O to *Nm*HO^X−PH−H_2O "aging"; low- and high-field portions of NOESY spectrum for *Nm*HO^X−PH-CN; and TOCSY spectrum for aromatic window) and one table (chemical shifts for *Nm*HO^X−PH−CN and *Nm*HO^A−PH−CN). This material is available free of charge via the Internet at http://pubs.acs.org.

REFERENCES

1. Zhu, W., Willks, A., and Stojiljkovic, I. (2000) Degradation of heme in gram-negative bacteria: the product of the hemO gene of *Neisseriae* is a heme oxygenase, *J. Bacteriol. 182*, 6783−6790.
2. Wilks, A., and Schmitt, M. P. (1998) Expression and characterization of a heme oxygenase (HmuO) from *Corynebacterium diphtheriae*, *J. Biol. Chem. 273*, 837−841.
3. Ratliff, M., Zhu, M., Deshmukh, R., Wilks, A., and Stojiljkovic, I. (2001) Homologues of Neisserial Heme Oxygenase in Gram-Negative Bacteria: Degradation of Heme by the Product of the pigA Gene of *Pseudomonas aeruginosa*, *J. Bacteriol. 183*, 6394−6403.
4. Yoshida, T., and Migita, C. T. (2000) Mechanism of heme degradation by heme oxygenase, *J. Inorg. Biochem. 82*, 33−41.
5. Wilks, A. (2002) Heme Oxygenase: Evolution, Structure, and Mechanism, *Antioxid. Redox Signaling 4*, 603−614.
6. Frankenberg-Dinkel, N. (2004) Bacterial Heme Oxygenases, *Antioxid. Redox Signaling 6*, 825−834.
7. Ishikawa, K., Sato, M., Ito, M., and Yoshida, T. (1992) Importance of histidine residue 25 of rat heme oxygenase for its catalytic activity, *Biochem. Biophys. Res. Commun. 182*, 981−986.
8. Wilks, A., and Demontellano, P. R. O. (1993) Rat Liver Heme Oxygenase−High Level Expression Of a Truncated Soluble Form and Nature Of the Meso-Hydroxylating Species, *J. Biol. Chem. 268*, 22357−22362.
9. Ortiz de Montellano, P. R., and Auclair, K. (2003) in *The Porphryin Handbook* (Kadish, K. M., Smith, K. M., and Guilard, R., Eds.) pp 175−202, Elsevier Science, San Diego, CA.
10. Ortiz de Montellano, P. R. (2000) The mechanism of heme oxygenase, *Curr. Opin. Chem. Biol. 4*, 221−227.
11. Ortiz de Montellano, P. R., and Wilks, A. (2001) Heme Oxygenase Structure and Mechanism, *Adv. Inorg. Chem. 51*, 359−407.
12. Rivera, M., and Zeng, Y. (2005) Heme Oxygenase, steering dioxygen activation toward heme hydroxylation, *J. Inorg. Biochem. 99*, 337−354.
13. Davydov, R. M., Yoshida, T., Ikeda-Saito, M., and Hoffman, B. M. (1999) Hydroperoxy-Heme Oxygenase Generated by Cryoreduction Catalyzes the Formation of α-*meso*-Hydroxyheme as Detected by EPR and ENDOR, *J. Am. Chem. Soc. 121*, 10656−10657.

14. Wang, J., and Ortiz de Montellano, P. R. (2003) The Binding Sites on Human Heme Oxygenase-1 for Cytochrome P450 Reductase and Biliverdin Reductase, *J. Biol. Chem. 278*, 20069−20076.
15. Unno, M., Matsui, T., Chu, G. C., Coutoure, M., Yoshida, T., Rousseau, D. L., Olson, J. S., and Ikeda-Saito, M. (2004) Crystal Structure of the Dioxygen-bound Heme Oxygenase from *Corynebacterium diphtheriae*, *J. Biol. Chem. 279*, 21055−21061.
16. Schuller, D. J., Wilks, A., Ortiz de Montellano, P. R., and Poulos, T. L. (1999) Crystal structure of human heme oxygenase-1, *Nature Struct. Biol. 6*, 860−867.
17. Lad, L., Wang, J., Li, H., Friedman, J., Bhaskar, B., Ortiz de Montellano, P. R., and Poulos, T. L. (2003) Crystal Structures of the Ferric, Ferrous and Ferrous-NO Forms of the Asp140Ala Mutant of Human Heme Oxygenase-1: Catalytic Implications, *J. Mol. Biol. 330*, 527−538.
18. Sugishima, M., Sakamoto, H., Higashimoto, Y., Omata, Y., Hayashi, S., Noguchi, M., and Fukuyama, K. (2002) Crystal structure of rat heme oxygenase-1 in complex with heme bound to azide: Implication for regiospecific hydroxylation of heme at the α-*meso* carbon, *J. Biol. Chem.* 45086−45090.
19. Sugishima, M., Sakamoto, H., Noguchi, M., and Fukuyama, K. (2003) Crystal Structures of CO-, CN-, and NO-Bound Forms of Rat Heme Oxygenase-1 (HO-1) in Complex with Heme: Structural Implications for Discrimination between CO and O2 in HO-1, *Biochemistry 42*, 9898−9905.
20. Schuller, D. J., Zhu, W., Stojiljkovic, I., Wilks, A., and Poulos, T. L. (2001) Crystal structure of heme oxygenase from the Gram-negative pathogen *Neisseria meningitidis* and a comparison with mammalian heme oxygeanse-1, *Biochemistry 40*, 11552−11558.
21. Friedman, J. M., Lad, L., Deshmukh, R., Li, H. Y., Wilks, A., and Poulos, T. L. (2003) Crystal structures of the NO- and CO-bound heme oxygenase from *Neisseriae meningitidis*—Implications for O2 activation, *J. Biol. Chem. 278*, 34654−34659.
22. Hirotsu, S., Chu, G. C., Unno, M., Lee, D.-S., Yoshida, T., Park, S.-Y., Shiro, Y., and Ikeda-Saito, M. (2004) The Crystal Structures of the Ferric and Ferrous Forms of the Heme Complex of HmuO, a Heme Oxygenase of *Corynebacterium diphtheriae*, *J. Biol. Chem. 279*, 11937−11947.
23. Friedman, J., Lad, L., Li, H., Wilks, A., and Poulos, T. L. (2004) Structural Basis for Novel δ-Regioselective Heme Oxygenation in the Opportunistic Pathogen *Pseudomonas aeruginosa*, *Biochemistry 43*, 5239−5245.
24. Sugishima, M., Migita, C. T., Zhang, X., Yoshida, T., and Fukuyama, K. (2004) Crystal structure of heme oxygenase-1 from cyanobacterium *Synechocystis* sp. PCC 6803 in complex with heme, *Eur. J. Biochem. 271*, 4517−4525.
25. Koenigs Lightning, L., Huang, H.-W., Moënne-Loccoz, P., Loehr, T. M., Schuller, D. J., Poulos, T. L., and Ortiz de Montellano, P. R. (2001) Disruption of an active site hydrogen bond converts human heme oxygenase-1 into a peroxidase, *J. Biol. Chem. 276*, 10612−10619.
26. Caignan, G. A., Deshmukh, R., Wilks, A., Zeng, Y., Huang, H.-W., Moenne-Loccoz, P., Bunce, R. A., Eastman, M. A., and Rivera, M. (2002) Oxidation of heme to β- and δ-biliverdin by *Pseudomonas aeruginosa* Heme Oxygenase as a Consequence of an Unusual Seating of the Heme, *J. Am. Chem. Soc. 124*, 14879−14892.
27. Hernández, G., Wilks, A., Paolesse, R., Smith, K. M., Ortiz de Montellano, P. R., and La Mar, G. N. (1994) Proton NMR Investigation of Substrate-bound Heme Oxygenase: Evidence for Electronic and Steric Contributions to Stereoselective Heme Cleavage, *Biochemistry 33*, 6631−6641.
28. Gorst, C. M., Wilks, A., Yeh, D. C., Ortiz de Montellano, P. R., and La Mar, G. N. (1998) Solution ^{1}H NMR investigation of the molecular and electronic structure of the active site of substrate-bound human heme oxygenase: the nature of the distal hydrogen bond donor to bound ligands, *J. Am. Chem. Soc. 120*, 8875−8884.
29. Li, Y., Syvitski, R. T., Chu, G. C., Ikeda-Saito, M., and La Mar, G. N. (2003) Solution ^{1}H NMR investigation of the active site molecular and electronic structures of the substrate-bound, cyanide-inhibited bacterial heme oxygenase from *C. diphtheriae*, *J. Biol. Chem. 279*, 6651−6663.
30. Liu, Y., Zhang, X., Yoshida, T., and La Mar, G. N. (2004) ^{1}H NMR characterization of the solution active site structure of substrate-bound, cyanide-inhibited heme oxygenase from Neisseria meningitidis; Comparison to crystal structures, *Biochemistry 43*, 10112−10126.
31. Zeng, Y., Deshmukh, R., Caignan, G. A., Bunce, R. A., Rivera, M., and Wilks, A. (2004) Mixed Regioselectivity in the Arg-177 Mutants of *Corynebacterium diphtheriae* Heme Oxygenase as a Consequence of in-Plane Heme Disorder, *Biochemistry 43*, 5222−5238.
32. Fujii, H., Zhang, X., and Yoshida, T. (2004) Essential Amino Acid Residues Controlling the Unique Regioselectivity of Heme Oxygenase in *Pseudomonas aeruginosa*, *J. Am. Chem. Soc. 126*, 4466−4467.
33. Li, Y., Syvitski, R. T., Auclair, K., Wilks, A., Ortiz de Montellano, P. R., and La Mar, G. N. (2002) Solution NMR characterization of an unusual distal H-bond network in the active site of the cyanide-inhibited, human heme oxygenase complex of the symmetric substrate, 2,4-dimethyldeuterohemin, *J. Biol. Chem. 277*, 33018−33031.
34. Syvitski, R. T., Li, Y., Auclair, K., Ortiz de Montellano, P. R., and La Mar, G. N. (2002) ^{1}H NMR detection of immobilized water molecules within a strong hydrogen-bonding network in the distal side of substrate-bound human heme oxygenase, *J. Am. Chem. Soc. 124*, 14296−14297.
35. La Mar, G. N., Satterlee, J. D., and de Ropp, J. S. (2000) in *The Porphyrins Handbook* (Kadish, K. M., Smith, K. M., and Guilard, R., Eds.) pp 185−298, Academic Press, San Diego.
36. Johnston, P. D., Figueroa, N., and Redfield, A. G. (1979) Real-time solvent exchange studies of the imino and amino protons of yeast phenylalanine transfer RNA by Fourier transform NMR, *Proc. Natl. Acad. Sci. USA 76*, 3130−3134.
37. Jeener, J., Meier, B. H., Bachmann, P., and Ernst, R. R. (1979) Investigation of Exchange Processes by Two-Dimensional NMR Spectroscopy, *J. Chem. Phys. 71*, 4546−4553.
38. Piotto, M., Sandek, V., and Sklenar, V. (1992) Gradient-tailored excitation for single quantum NMR spectroscopy of aqueous solutions, *J. Biomol. NMR 2*, 661−666.
39. Griesinger, C., Otting, G., Wüthrich, K., and Ernst, R. R. (1988) Clean TOCSY for ^{1}H Spin System Identification in Macromolecules, *J. Am. Chem. Soc. 110*, 7870−7872.
40. Bax, A., and Davis, D. G. (1985) Mlev-17-based two-dimensional homonuclear magnetization transfer spectroscopy, *J. Magn. Reson. 65*, 355−360.
41. Zhang, X., Fujii, H., Matera, M., Migita, C. T., Sun, D., Sato, M., Ikeda-Saito, M., and Yoshida, T. (2003) Stereoselectivity of each of the three steps of the heme oxygenase reaction: hemin to *meso*-hydroxyhemin, *meso*-hydroxyhemin to verdoheme, and verdoheme to biliverdin, *Biochemistry 42*, 7418−7426.
42. Liu, Y., Zhang, X., Yoshida, T., and La Mar, G. N. (2005) Solution ^{1}H NMR characterization of the distal H-bond network and the effective axial field in the resting-state, high-spin ferric, substrate-bound complex of heme oxygenase from *N. meningitidis*, *J. Am. Chem. Soc. 127*, 6409−6422.
43. Wagner, G., Pardi, A., and Wüthrich, K. (1983) Hydrogen Bond Length and ^{1}H NMR Chemical Shifts in Proteins, *J. Am. Chem. Soc. 105*, 5948−5949.
44. Li, Y., Syvitski, R. T., Auclair, K., Ortiz de Montellano, P. R., and La Mar, G. N. (2003) Solution ^{1}H, ^{15}N NMR spectroscopic characterization of substrate-bound cyanide-inhibited, human heme oxygenase: water occupation of the distal cavity, *J. Am. Chem. Soc. 125*, 13392−13403.
45. Zhu, W., Wilks, A., and Stojiljkovic, I. (2000) Degradation of Heme in Gram-Negative Bacteria: the Product of the hemO Gene of *Neisseriae* Is a Heme Oxygenase, *J. Bacteriol. 182*, 6783−6790.
46. Yoshida, T., and Kikuchi, G. (1978) Features of the reaction of heme degradation catalyzed by the reconstituted microsomal heme oxygenase system, *J. Biol. Chem. 253*, 4230−4236.
47. Li, Y., Syvitski, R. T., Auclair, K., Ortiz de Montellano, P. R., and La Mar, G. N. (2003) 1H NMR Investigation of the Solution Structure of Substrate-free Human Heme Oxygenase: Comparison to the Cyanide-inhibited, Substrate-bound Complex, *J. Biol. Chem. 279*, 10195−10205.
48. Englander, S. W., and Kallenbach, N. R. (1984) Hydrogen exchange and structural dynamics of proteins and nucleic acids, *Q. Rev. Biophys. 16*, 521−655.

BI0523097